RSC Advances

PAPER

View Article Online
View Journal | View Issue

Cite this: *RSC Adv.*, 2025, **15**, 30378

Preparation of natural polymer-based hydrogels for oral delivery of anti-malarial drug: *in vitro* and cytotoxicity evaluation

Muhammad Suhail,[abc] Abdul Wahab,[ab] Guiyue Wang,[ab] Susu An,[ab] Bushra Kiran,[ab] Naila Jabeen,[ab] M. Zubair Iqbal, *[ab] Xiangdong Kong *[ab] and Pao-Chu Wu *[cde]

The current investigation involved the fabrication of gelatin-based hydrogels for controlled delivery of quinine. Hence, pH-responsive and biocompatible hydrogels were developed using natural polymer gelatin and synthetic monomer acrylic acid. The drug-loaded hydrogels indicated a new carrier system, which was confirmed by various physicochemical characterizations, including FTIR, TGA, DSC, and XRD, whereas SEM revealed the morphology of unloaded and drug-loaded hydrogels, respectively. Similarly, sol–gel and porosity studies were conducted to assess the soluble, insoluble, and fluid penetration across the prepared network. A significant increase in gelation, whereas a decline in sol fraction was detected with high hydrogel contents. Unlike gel fraction, a decline was observed with high integration of gelatin and *N*′,*N*′-methylene bisacrylamide, while acrylic acid showed the same effects as gel fraction on the porosity of the polymeric matrix. Swelling and drug release investigations confirmed the pH-dependent release of quinine at various simulated pH values of 1.2, 4.6, and 7.4, respectively. Both swelling and drug release showed a high swelling index and release of the drug from the fabricated hydrogel at higher pH values compared to lower pH values. Similarly, drug loading was conducted by a swelling and diffusion approach. The effects of acrylic acid, gelatin, and *N*′,*N*′-methylene bisacrylamide were the same on swelling, drug loading, and release as porosity. The biodegradation study revealed that high polymer, monomer, and crosslinker concentrations led to a slow hydrogel degradation. Furthermore, the developed matrix was subjected to cytotoxicity and cell viability studies on mouse fibroblast L929 cells, which indicated safe utilization of polymeric hydrogels with negligible toxicity. Hence, the strategy of preparing pH-responsive hydrogels of gelatin facilitates the controlled delivery of quinine for a prolonged time in order to overcome the challenges of quinine generated after its multiple intakes.

Received 16th June 2025
Accepted 6th August 2025

DOI: 10.1039/d5ra04256a

rsc.li/rsc-advances

1. Introduction

Hydrogels have emerged as one of the most significant classes of biomaterials due to their unique structural and functional features. These materials are characterized by a highly porous, three-dimensional network of crosslinked polymers capable of holding a substantial amount of aqueous or biological fluids, typically exceeding 20% of their total mass. Owing to the nature of their chemical and physical interactions.[1–4] These networks remain stable without dissolving, making hydrogels suitable for various biomedical applications. Their high water holding capability imparts excellent biocompatibility and enables efficient encapsulation and controlled release of hydrophilic therapeutic agents.[5] Additionally, their compositional versatility and adaptability allow for administration *via* multiple routes, including parenteral (*e.g.*, intramuscular, intradermal) and non-parenteral (*e.g.*, topical, oral) pathways.[6]

Recent advances have focused on the development of stimuli-responsive hydrogels as drug delivery systems (DDSs). These smart systems release therapeutic substances in response to internal or external stimuli, offering spatial and temporal control over the release of the drug. Compared to conventional delivery methods, such systems offer greater therapeutic efficacy and lower systemic toxicity.[7] Stimuli are broadly categorized into exogenous (*e.g.*, light, magnetic fields, ultrasound) and endogenous (*e.g.*, pH, temperature, enzymatic activity) types. Among these, pH-responsive systems are particularly promising, as they exploit variations in acidity across different

[a]*Institute of Smart Biomedical Materials, School of Materials Science and Engineering, Zhejiang Sci-Tech University, Hangzhou, 310018, China*
[b]*Zhejiang-Mauritius Joint Research Center for Biomaterials and Tissue Engineering, Zhejiang Sci-Tech University, Hangzhou, 310018, China*
[c]*School of Pharmacy, Kaohsiung Medical University, 100 Shih-Chuan 1st Road, Kaohsiung, 80708, Taiwan*
[d]*Department of Medical Research, Kaohsiung Medical University Hospital, Kaohsiung, 80708, Taiwan*
[e]*Drug Development and Value Creation Research Center, Kaohsiung Medical University, Kaohsiung, 80708, Taiwan*

physiological environments, most notably in pathological sites such as tumor tissues. By leveraging these localized pH differences, pH-sensitive hydrogels enable targeted drug release, minimizing adverse effects and maximizing therapeutic outcomes.[8,9]

Gelatin (GLTN), a denatured protein derived from collagen, is employed highly in hydrogel formation due to its biocompatibility, biodegradability, and excellent gelation behavior. It exists in two forms: type A (cationic, derived from pig skin) and type B (anionic, derived from bovine collagen *via* alkaline hydrolysis).[10,11] GLTN can interact with hydrophobic and hydrophilic drugs, making it a versatile matrix for drug delivery.[12,13] Acrylic acid (ACAD), a pH-sensitive, water-soluble monomer with extensive biomedical applications, can be combined with polymer to develop polymeric hydrogels, exhibiting precise and responsive drug release behavior. ACAD-based hydrogels, such as carbopol, are known to swell significantly under alkaline pH conditions, facilitating controlled drug release in environments like the intestine or tumor extracellular matrix.[14]

Quinine (Qn), a naturally occurring alkaloid extracted from the bark of *Cinchona* species, has long been used as a therapeutic agent against malaria. It is particularly effective against the asexual blood stages of *Plasmodium falciparum*, especially in chloroquine-resistant strains. Qn is currently administered orally or intravenously; intramuscular injection is discouraged due to the risk of abscess formation and intense pain. The half-life of Qn is 11 h, and thus absorbed very rapidly. Plasma protein binding affinity is very high. Its short half-life necessitates frequent dosing, which is associated with a range of adverse effects such as hypoglycemia, gastrointestinal distress, cinchonism (manifesting as vertigo, tinnitus, deafness, and headache), hypotension, cardiac arrhythmias, neuropsychiatric disturbances, leukopenia, erythema, bradycardia, methemoglobinemia, and hemolysis.[15,16] Therefore, a carrier system is needed to overcome Qn-associated adverse effects after its administration and improve patient compliance. Dandagi *et al.* prepared solid lipid nanoparticles and sustained the release of quinine for 1.5 h.[17] Similarly, Kesse and coworkers reported controlled release of quinine by fabricated microspheres up to 24 h.[18] Despite this, much work remains to overcome the challenges faced by quinine administration. Hence, the authors developed natural polymer-based pH-responsive gelatin hydrogels for the controlled release of Qn.

In the current study, a pH-sensitive hydrogel network was fabricated to control Qn release and minimize the associated side effects. The pH-sensitivity was increased by incorporating a pH-responsive ACAD, which showed excellent computability with GLTN. The fabricated polymeric matrix limited Qn absorption in the upper parts of the gastrointestinal tract. The developed matrices were exposed to various *in vitro* characterizations, such as SEM, FTIR, TGA, DSC, and XRD. Similarly, porosity, drug release, sol–gel, and swelling studies were performed for the prepared hydrogels. Furthermore, biodegradation and cytotoxicity studies were conducted, which indicated excellent biocompatibility and negligible cytotoxicity of the designed hydrogel networks.

2. Experimental

2.1 Materials

N′,*N*′-Methylene bisacrylamide (MBA) was purchased from Rhawn, China. GLTN was obtained from Shanghai MacLean Biochemical Technology Co., Ltd., China. Similarly, Qn, ACAD, and ammonium persulfate (Aps) were bought from General Reagent, Shanghai Titan Technology Co., Ltd., China. Mouse fibroblast L929 cells were purchased from ATCC 10801 University Boulevard Manassas, VA 20110-2209, USA.

2.2 Synthesis of gelatin/acrylic acid (GLTN/ACAD) hydrogel

The GLTN/ACAD hydrogels were developed by a free radical polymerization approach. Initially, a measured amount of GLTN was dissolved in deionized water at 80 °C with continuous stirring using a magnetic stirrer to ensure complete solubilization. Aps was dissolved in a minimal volume of water in a separate beaker. ACAD was introduced dropwise into the GLTN solution, and then Aps was gradually added, maintaining uniform agitation until a homogeneous mixture was achieved. In parallel, the crosslinker solution was prepared by dissolving MBA in a water/ethanol mixture, stirring at 50 °C. After 20 minutes of mixing on a heated magnetic stirrer, the crosslinker solution was poured slowly into the aforementioned mixture. Stirring was continued till the solution attained complete clarity, indicating uniform dispersion of all reactants. The resulting reaction mixture was transferred into cylindrical glass moulds, sealed to prevent contamination, and placed at 50 °C in a preheated oil bath for an initial polymerization phase of 2 h. Subsequently, the temperature was elevated to 60 °C and maintained for 24 h to ensure complete crosslinking. Upon completion, the hydrogel cylinders were removed, cooled to room temperature, and sectioned into uniform discs (8 mm diameter). The discs were washed repeatedly with ethanol and positioned in a vacuum oven at 40 °C to dry for 168 h. Different hydrogel compositions were prepared to investigate the various formulation effects by altering the concentrations of GLTN, ACAD, and MBA, while keeping other synthesis conditions constant. Formulation and proposed chemical structure are indicated in Table 1 and Fig. 1.

2.3 Structural analysis, sol–gel/porosity/and swelling studies

Fourier-transform infrared (FTIR) spectroscopy, thermogravimetric analysis (TGA), differential scanning calorimetry (DSC), X-ray diffraction (XRD), scanning electron microscopy (SEM), sol–gel, porosity, and swelling studies were performed according to previous publications.[19,20]

2.4 Polymer volume fraction (PVF)

To assess the extent of polymer concentration in the swollen hydrogel matrix, PVF was calculated at pH 1.2, 4.6, and 7.4.[21] The equilibrium swelling volume (V_{eq}) was measured, and PVF was determined using;

$$\mathrm{PVF} = \frac{1}{V_{eq}} \quad (1)$$

Table 1 Formulation ratios of GLTN/ACAD hydrogels

Formulation code	Polymer (GLTN) g/100 g	Monomer (ACAD) g/100 g	Initiators (Aps) g/100 g	Cross-linker (MBA) g/100 g
GF-1	1.00	26.0	0.32	0.65
GF-2	1.34	26.0	0.32	0.65
GF-3	1.68	26.0	0.32	0.65
GF-4	0.66	28.5	0.32	0.65
GF-5	0.66	30.5	0.32	0.65
GF-6	0.66	32.5	0.32	0.65
GF-7	0.66	26.0	0.32	0.72
GF-8	0.66	26.0	0.32	0.78
GF-9	0.66	26.0	0.32	0.84

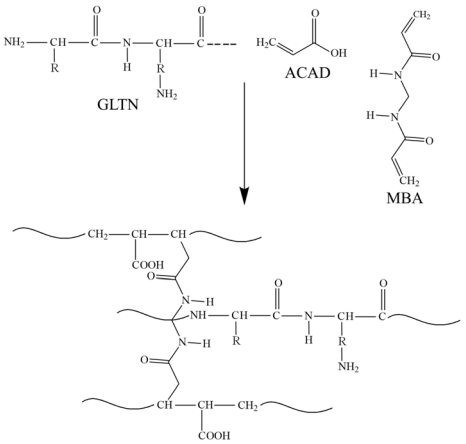

Fig. 1 Proposed chemical structure of GLTN/ACAD hydrogel.

The polymer's volume fraction is denoted as PVF. The equilibrium swelling volume is denoted as V_{eq}.

2.5 Biodegradation study

In vitro degradation was assessed in phosphate-buffered saline (PBS, pH 7.4) at 37 °C. Pre-weighed dried hydrogel discs were incubated in PBS for various intervals. After each time point, the samples were removed, vacuum-dried to a constant weight,[22,23] and the degradation percentage was calculated using:

$$D = (S_1 - S_2)/S_1 \times 100 \quad (2)$$

In this equation, D represents degradation. The weight of the sample when dried is denoted as S_1, while hydrogel weight after immersion, denoted as time (t), is represented by S_2.

2.6 Drug loading

Drug incorporation was achieved using an equilibrium diffusion technique. A 1% w/v Qn solution was prepared by dissolving quinine in phosphate buffer (pH 7.4) with continuous magnetic stirring at ambient temperature to ensure complete solubilization. Pre-weighed hydrogel discs from each formulation batch were immersed in the drug solution and maintained under static conditions for 24 h to facilitate passive diffusion of the drug into the polymer matrix. After loading, the discs were gently rinsed with deionized water to remove any non-entrapped surface drug and dried in a vacuum oven.

To determine the loaded drug content, Qn was extracted by immersing drug-loaded hydrogel discs in pH 7.4 (40 mL). Samples were reserved at designated time points and substituted with new media to ensure full extraction. A UV-spectrophotometer (MAPADA instrument) was utilized in order to determine the absorbance of the collected samples at λ_{max} 207 nm. All tests were performed in triplicate to ensure precision.[24]

2.7 Drug release content

Drug release was evaluated from the hydrogels utilizing a USP type II dissolution apparatus in the same swelling buffer solutions. Each disc was put in 900 mL of the medium at 37 ± 0.5 °C and 50 rpm. At designated intervals, 5 mL aliquots were extracted and replaced with fresh buffer. The Qn concentration in the samples was determined using a UV spectrophotometer (MAPADA instrument) at a wavelength of 207 nm. The obtained data were fitted to various kinetic models to analyse the release mechanism.[25]

2.8 Cytotoxicity study

Hydrogel formulations were tested for cytotoxicity on mouse fibroblast L929 cells (ATCC 10801 University Boulevard Manassas, VA 20110-2209, USA) using the Cell Counting Kit-8 (CCK-8) assay. To facilitate cell adhesion, cells were seeded onto 96-well plates at a density of 1×10^5 cells per well and incubated at 37 °C in a humidified incubator with 5% CO_2 for 24 hours. After that, fresh culture media with sterilized hydrogel samples at 5–20 mg mL^{-1} were added. Following a 24 hours incubation period, 10 μL of CCK-8 reagent was added to each well and incubated for two more hours. A microplate reader assessed absorbance at 450 nm and evaluated cell viability relative to untreated control wells.[26,27]

$$\text{Formula: } (OD_{sample} - OD_{Black})/(OD_{control} - OD_{Black}) \times 100 \quad (7)$$

To substantiate these findings, live cell staining was conducted utilizing Calcein-AM dye. L929 cells, at a density of 2×10^5 cells per well, were seeded in 24-well plates that contained sterilized hydrogel discs. After 24 hours of incubation, the

culture media was removed and the cells were gently washed with PBS. Subsequently, a 2 μM Calcein-AM solution was added to each well, with a further incubation period of 30 minutes at 37 °C. Excess dye was eliminated by rinsing with PBS, and the samples were examined under a fluorescence microscope to visualize viable cells adhering to the hydrogel surface.[28]

2.9 Statistical analysis

All experimental data were analyzed using SPSS 22.0 (IBM Corp., Armonk, NY, USA). The results are shown as mean ± standard deviation. Student's *t*-test compared groups. Statistical significance was defined as a p-value < 0.05.

3. Results and discussion

3.1 Synthesis of GLTN/ACAD hydrogels

GLTN/ACAD hydrogels were synthesized *via* free radical polymerization employing GLTN as the polymer backbone, whereas ACAD and MBA were used as monomer and cross-linking agent. Various concentrations of GLTN were used to tailor the hydrogel properties. The resulting hydrogels exhibited a uniform, partially porous network structure with adequate mechanical integrity and gelling characteristics. The hydrogels appeared light yellow (Fig. 2A) in color. Each formulation began as a transparent homogeneous reaction mixture before gelation, indicating efficient solubilization and mixing of the reactants.

3.2 Structural analysis

FTIR spectroscopy confirmed the chemical structure and assessed cross-linking in the fabricated hydrogels. FTIR analysis was performed for GLTN, ACAD, Qn, unloaded, and drug-loaded GLTN/ACAD hydrogels (Fig. 2B). The FTIR of pure GLTN exhibited characteristic bands at 3278 cm^{-1} (N–H stretching), 1632 cm^{-1} (C=O stretching, amide I), and 1530 cm^{-1} (C–N bending, amide II), consistent with literature reports.[29] ACAD's FTIR spectra exhibited peaks at 2973 and 1709 cm^{-1}, corresponding to the stretching vibrations of $-CH_2-$ and the carboxyl group. The peaks at 1639 and 1299 cm^{-1} proved the presence of C=O and C–C stretching, respectively. Similarly, the C–O stretching vibration was indicated by a peak at 1172 cm^{-1}.[30] FTIR spectra of GLTN/ACAD hydrogel showed polymer and monomer peaks of different intensities. The GLTN and ACAD peaks at 2973, 1639 cm^{-1}, and 1299, 1172 cm^{-1} were shifted to the hydrogel's peaks at 2950, 1620, 1310, and 1205 cm^{-1}. Certain peaks appeared and some disappeared. All of this suggests the formation of a hydrogel matrix. FTIR analysis of Qn displayed prominent bands at 3372 cm^{-1} (O–H stretching), 2860–2918 cm^{-1} (C–H stretching), and bands at 1078, 1240, and 1622 cm^{-1} representing C–N, C=O, and C=C stretching,[31,32] correspondingly. In the FTIR spectrum of drug-loaded hydrogels, distinct shifts and suppression of peaks in the 1000–1600 cm^{-1} region, along with a new peak at 1172 cm^{-1}, confirmed cross-linking and drug incorporation.[33]

TGA was performed to assess the thermal stability of the pure components and the cross-linked hydrogel formulation, as presented in Fig. 2C. The TGA thermogram of GLTN displayed an initial loss of 10% in weight at 250 °C, attributed to moisture evaporation. Onward temperature of up to 400 °C caused a 50% reduction in weight. After that, complete degradation of GLTN occurred with further increase in temperature.[29] In contrast, the hydrogel formulation showed enhanced thermal stability, with the first mass reduction of 7% at 250 °C because of moisture loss. A secondary degradation event started at 280 °C, and almost 22% mass reduction was detected at 322 °C. A final major weight loss of 50% at 500 °C was observed. This all indicates the formation of a more stable polymeric network. B. Singh and co-workers also stated the same results for the prepared hydrogel,[34] as in our investigation. Similarly, at 350 and 450 °C temperatures, the TGA of Qn demonstrated a mass loss of 30 and 32%, respectively. A further mass loss led to Qn degradation with the increasing temperature. The drug-loaded GLTN/ACAD hydrogel exhibited a marginally higher stability than the unloaded hydrogel, which was attributed to the presence of the drug.[35]

DSC thermograms were carried out for the aforementioned samples, as indicated in Fig. 2D. The pure gelatin exhibited an endothermic peak at 110 °C (water loss), followed by two other minor endothermic peaks at 220 and 270 °C. A major exothermic peak was seen at 245 °C.[36] In comparison, the hydrogel formulation showed a first endothermic peak at 70 °C, whereas the second endothermic peak was seen at 200 °C, which were the peaks of GLTN moved from 110 and 220 °C after crosslinking. Similarly, an exothermic peak was detected at 225 °C, shifted from GLTN. The presence of GLTN peaks in the fabricated hydrogel indicated the preparation of a thermally stable cross-linked polymeric system. Bucak and co-workers stated the same results[37] as in our findings, which strengthened our investigation further. The DSC profile of Qn revealed a broad desolvation peak at 64 °C and a sharp melting endotherm peak at 175 °C.[31] The slight alterations in the peaks of Qn signified the effective incorporation of Qn into the hydrogel matrix. Because of the presence of the drug, the DSC profile of

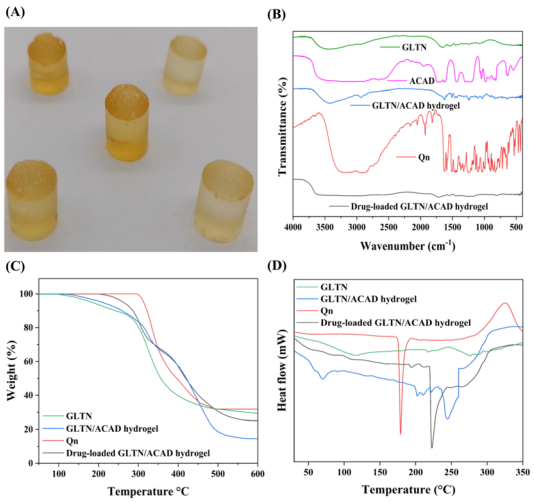

Fig. 2 (A) Physical appearance, (B) FTIR, (C) TGA, and (D) DSC of GLTN, ACAD, GLTN/ACAD hydrogel, Qn, and drug-loaded GLTN/ACAD hydrogel.

the drug-loaded GLTN/ACAD hydrogel differed slightly from unloaded hydrogel.[35]

XRD analysis was conducted to investigate the crystallinity of GLTN, Qn, and both blank and drug-loaded hydrogels, as illustrated in Fig. 3. Pure GLTN exhibited small crystalline peaks at 2θ = 20.12°, 30.31°, and 40.62°, which diminished in the blank hydrogel, indicating reduced crystallinity due to successful cross-linking. The XRD of Qn showed numerous sharp peaks at 2θ values of 11.12°, 15.91°, 16.14°, 17.35°, 18.41°, 19.63°, 20.01°, 24.14°, and 25.83 *etc.*, confirming its crystalline nature.[31] In the drug-loaded hydrogels, these crystalline peaks were significantly reduced, suggesting partial drug amorphization upon entrapment in the hydrogel matrix. The similarity in XRD patterns between unloaded and loaded hydrogels, with minor peak shifts, further supports successful drug encapsulation without altering the hydrogel's structural framework. Interestingly, our findings are quite matching with the results reported by Lee and coworkers in their previous investigation.[38]

SEM analysis of the GLTN/ACAD hydrogel revealed a hard surface morphology with a few pores (Fig. 4A) attributed to the successful cross-linking of GLTN with ACAD. The porous microstructure facilitates water diffusion throughout the hydrogel matrix, enhancing its swelling behavior and drug release potential in aqueous environments. The hard structure of the polymeric hydrogel may be attributed to the viscosity of GLTN. The water penetration occurred through the spores, allowing the hydrogel network to swell and *vice versa*. The SEM of drug-loaded GLTN/ACAD hydrogel (Fig. 4B) indicated a more viscous network than the unloaded hydrogel due to the presence of the drug. Thus, the drug is released slowly and gradually from the viscous hydrogel network in a controlled fashion.[39]

3.3 Sol–gel fraction

The sol–gel fraction was evaluated to determine the extent of cross-linking during free radical polymerization. GLTN, ACAD, and MBA contents influenced both gel and sol fractions, as presented in Fig. 5A–C. As concentrations of GLTN and ACAD were increased, a corresponding increase in gel fraction was observed. Because of the presence of a significant number of free radicals, the polymerization between GLTN and ACAD contents was enhanced with their increasing concentrations. The polymerization occurred rapidly as the contents of GLTN and ACAD increased. Similarly, high MBA integration resulting in improved polymerization efficiency. The gelation among hydrogel contents increased with the high MBA concentration, and thus, a high dense hydrogel network was formed. All hydrogel formulations exhibited gel fractions exceeding 90%, demonstrating high cross-linking. This is attributed to the availability of more reactive sites at higher concentrations of the monomer and cross-linker, enhancing network formation. These findings are consistent with Ranjha *et al.*, who reported increased gel fractions with elevated MBA concentrations in CS/AA hydrogels.[40] On the other hand, high gelation caused a reduction in the hydrogel sol fraction because of an inverse relation. Thus, high GLTN, ACAD, and MBA contents resulted in a decrease of sol-fraction.[41]

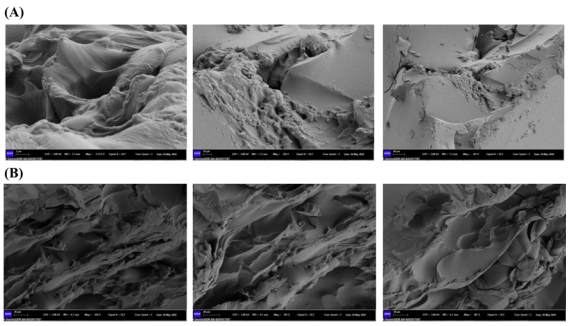

Fig. 4 SEM of (A) unloaded and (B) drug-loaded GLTN/ACAD hydrogel.

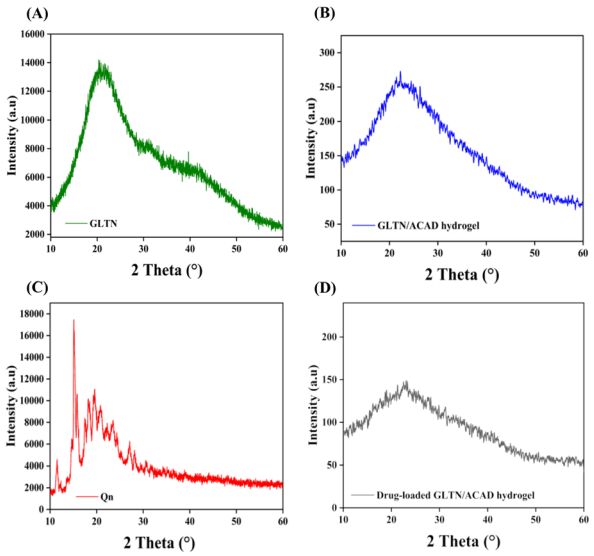

Fig. 3 XRD of (A) GLTN, (B) GLTN/ACAD hydrogel, (C) Qn, and (D) drug-loaded GLTN/ACAD hydrogel.

3.4 Porosity study

Porosity plays a crucial role in modulating the swelling behavior, drug loading, and release characteristics of hydrogels. Typically, higher porosity correlates with greater swelling and drug release capacities. Therefore, the porosity of prepared

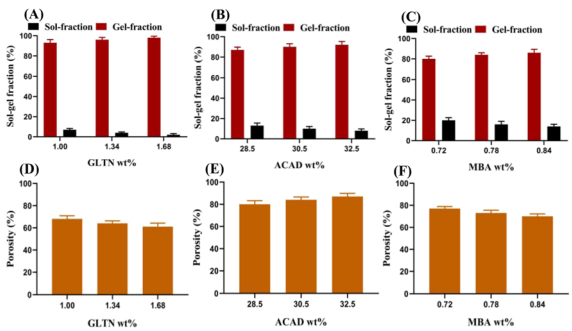

Fig. 5 Effects of GLTN, ACAD, and MBA on (A–C) sol–gel fraction and (D–F) porosity of GLTN/ACAD hydrogel.

matrices was assessed to evaluate their fluid penetration capabilities. The GLTN/ACAD hydrogel contents highly affected the porosity (Fig. 5D–F). The porosity of the polymeric matrix was enhanced with high ACAD contents. This may be correlated with increasing viscosity during polymerization, which impeded bubble escape and promoted the formation of interconnected channels. These channels are responsible for fluid penetration across the hydrogel network. In contrast, higher concentrations of GLTN and MBA produced denser networks, reducing porosity due to restricted polymer chain mobility. The crosslinking and bulkiness of the carrier system were enhanced with the increasing GLTN and MBA contents. Therefore, a decline in fluid penetration was seen with high polymer and crosslinker contents. Thus, low porosity and swelling were ultimately achieved.[42]

3.5 Swelling and drug release studies

Swelling behavior and drug release profiles of GLTN/ACAD hydrogels were evaluated at pH 1.2, 4.6, and 7.4, as shown in Fig. 6A and 7A. All formulations exhibited greater swelling at high pH (7.4), leading to high drug release because of carboxylic groups (COOH → COO^-) ionization of GLTN and ACAD above the pK_a (~4.28), resulting in electrostatic repulsion and matrix expansion. The repulsive forces were generated as a result of the greater charge density of similar functional groups. These repulsive forces among hydrogel contents led to high swelling, which led to maximum drug release, correspondingly. The low swelling and release behavior at low pH correlated with conjugate formation of the GLTN and ACAD contents with counter ions by strong hydrogen bonds, which caused a low swelling and drug release ultimately.[43] The low swelling and drug release at low pH indicate the pH-responsive nature of the developed hydrogel, which not only sustains the release of the drug but also protects the drug from degradation in the acidic media. Similarly, the upper parts, particularly the stomach of the gastrointestinal tract, are protected from the drug's adverse effects. Thus, it can be conceded that the prepared hydrogel matrix sustained the release of Qn in a controlled pattern.

GLTN, ACAD, and MBA greatly affected both swelling and drug release of formulated GLTN/ACAD hydrogels, as indicated in Fig. 6B–D and 7B–E. Increased ACAD concentration led to higher swelling and drug release across the pH range, consistent with increased ionization and hydrophilicity.[44] Unlikely, formulations with increased GLTN content showed reduced swelling and drug release across all pH values due to high crosslinking, and the influence of GLTN isoelectric point.[29] Similarly, hydrogels with higher MBA content reduced swelling and drug release due to tighter network formation, which limited solvent uptake and drug diffusion. These observations reflect the balance between polymer hydrophilicity, cross-linking density, and the dynamic behavior of polymer chains in aqueous media.[45] The release data of Qn were fitted to all kinetic models. Among these, the first order best described the drug release kinetics, as evidenced by the highest regression coefficients (r^2) (Table 2). All formulations' calculated release exponent values (n > 0.45) indicated non-Fickian diffusion.[46]

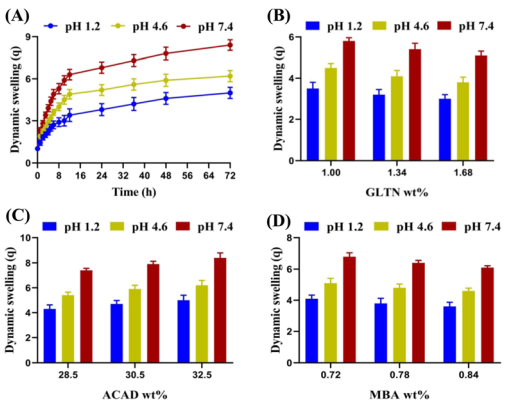

Fig. 6 Influence of (A) pH, (B) GLTN, (C) ACAD, and (D) MBA on dynamic swelling of GLTN/ACAD hydrogel.

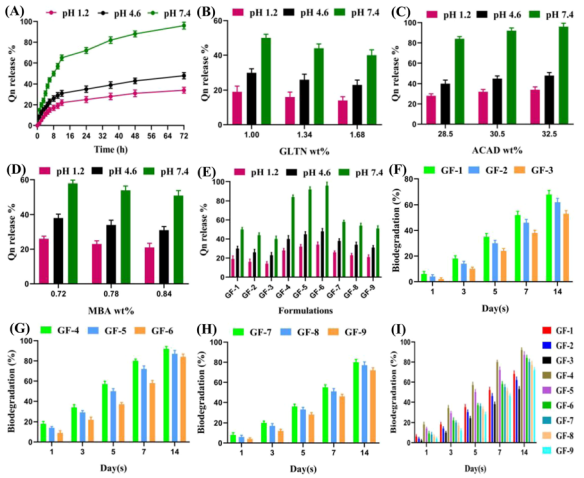

Fig. 7 Effects of pH, GLTN, ACAD, and MBA on (A–E) drug release and (F–I) biodegradation of GLTN/ACAD hydrogel.

3.6 PVF

The PVF was determined at pH 1.2, 4.6, and 7.4 to evaluate the extent of polymeric content in the swollen state of the hydrogels, as indicated in Table 3. A higher PVF was observed at pH

Table 2 Release mechanism and order of Qn from GLTN/ACAD hydrogels

F. code	Zero order r^2	First order r^2	Higuchi r^2	Korsmeyer–Peppas r^2	Korsmeyer–Peppas n
GF-1	0.9513	0.9880	0.9592	0.9677	0.5245
GF-2	0.9023	0.9930	0.9313	0.9831	0.5412
GF-3	0.9334	0.9816	0.9611	0.9543	0.5808
GF-4	0.9616	0.9772	0.9227	0.9525	0.5520
GF-5	0.9243	0.9850	0.9761	0.8945	0.5317
GF-6	0.9517	0.9992	0.9820	0.9868	0.6024
GF-7	0.9825	0.9856	0.9119	0.9382	0.6176
GF-8	0.9902	0.9932	0.9672	0.9506	0.6420
GF-9	0.8920	0.9910	0.8803	0.9210	0.5731

1.2, whereas lower values were recorded at pH 4.6 and 7.4, indicating an inverse relationship between swelling capacity and PVF (formula (1)). Increase in swelling leads to decrease in PVF, and *vice versa*. This trend is attributed to the enhanced ionization of carboxylic groups at higher pH levels, leading to increased swelling and reduced PVF. Increasing the concentration of GLTN and MBA elevated the PVF due to denser network formation, while higher ACAD concentrations decreased PVF due to expanded matrix swelling.[21]

3.7 Biodegradation study

The biodegradability of the GLTN/ACAD hydrogels was assessed under simulated physiological conditions. Like other studies, hydrogel contents also influenced the biodegradation rate of the polymeric hydrogels, as illustrated in Fig. 7F–I. The fabricated hydrogel matrix exhibited slower degradation rates with increasing concentrations of ACAD. This may be correlated with the increasing functional groups of ACAD, which led to fast polymerization and crosslinking. Similarly, GLTN and MBA forming a highly cross-linked network that limits hydrolytic cleavage. Higher levels of such reactants enhanced free radical generation during polymerization, facilitating rapid gelation and the development of a dense, mechanically robust matrix. These hydrogel contents decreased pore size of the hydrogel matrix, which retarded enough water penetration, and thus, as a result, low porosity, swelling, and drug loading were achieved with their increasing contents. On the other hand, a low biodegradation rate of the polymeric hydrogel was achieved due to tight junctions, and *vice versa*. These findings align with Mohamed and coworkers, who reported reduced degradation in chitosan/PVA-based hydrogels with elevated feed ratios due to similar network stabilization effects.[47]

3.8 Drug loading

The loading of Qn by the formulated matrix was affected by the hydrogel contents (Table 3). Drug loading efficiency was inversely correlated with growing concentrations of GLTN and MBA, whereas ACAD showed a direct effect. Increased GLTN and MBA contents led to higher cross-linking densities, resulting in a tighter polymeric network with limited free volume, which hindered drug entrapment. Conversely, higher ACAD concentrations promoted swelling and porosity, facilitating greater drug incorporation.[48] These results are consistent with those of Sairam *et al.*, who observed reduced drug loading in polyacrylamide hydrogels with elevated MBA levels due to the formation of compact, less permeable matrices.[49]

Table 3 PVF and drug loading of GLTN/ACAD hydrogels

F. code	PVF pH 1.2	PVF pH 4.6	PVF pH 7.4	Drug loaded (mg) extraction method
GF-1	0.285	0.222	0.171	148.43 ± 1.32
GF-2	0.312	0.243	0.185	140.51 ± 0.84
GF-3	0.333	0.263	0.196	136.13 ± 0.63
GF-4	0.232	0.188	0.135	170.24 ± 1.80
GF-5	0.212	0.169	0.126	179.30 ± 0.72
GF-6	0.200	0.161	0.119	184.63 ± 0.34
GF-7	0.243	0.196	0.147	166.82 ± 1.04
GF-8	0.263	0.208	0.156	160.53 ± 0.21
GF-9	0.277	0.217	0.163	156.26 ± 1.90

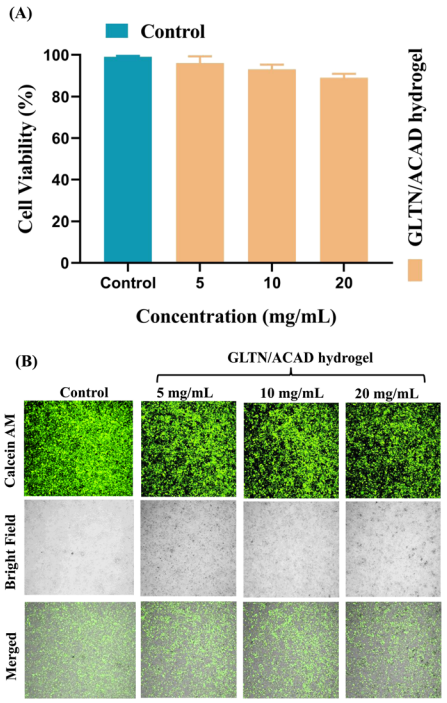

Fig. 8 (A) Cytotoxicity and (B) effects of different hydrogel concentrations on the viability of L929 cells.

3.9 Cytotoxicity study

The toxicity of the prepared hydrogels was evaluated using the CCK-8 assay to assess the viability of L929 cells, as indicated in Fig. 8A. Cytotoxicity studies are essential for identifying any toxic effects of materials intended for pharmaceutical and biomedical applications. According to the literature, materials are considered non-cytotoxic if cell viability exceeds 70% compared to a blank control. The current study showed that the hydrogel's cell viability was greater than 85% after 24 h of incubation, indicating that the hydrogels exhibited no cytotoxic effects at varying concentrations. Consequently, the fabricated networks are deemed safe for potential clinical applications.[50]

To further evaluate cell proliferation, L929 cells were stained with Calcein AM and incubated on hydrogel surfaces for 24 h. Fluorescent microscopy images revealed green fluorescence corresponding to live cells, with many viable cells observed on all hydrogel concentrations (Fig. 8B). This suggests that the hydrogels promote excellent cell growth, surface spreading, and proliferation, indicating their biocompatibility and negligible toxicity. These results support the potential of the hydrogels for future clinical use with minimal risk of cytotoxicity.[28]

4. Conclusions

The development, thermal stability, and crystallinity of GLTN/ACAD hydrogels were evaluated by FTIR, TGA, DSC, and XRD

analysis. These physicochemical characterizations confirmed successful preparation, an increase in thermal behavior of GLTN, and a reduction in crystallinity of GLTN and drug by polymeric hydrogels. The hard surface of the prepared matrix with tiny pores was demonstrated by SEM. The measurement of sol and gel fractions was carried out by sol–gel analysis. A low sol fraction was observed with increasing concentration of hydrogel contents, whereas gel fraction showed the reverse effect to sol fraction. The influence of GLTN, ACAD, and MBA on swelling, porosity, drug loading, and release was found same. The aforementioned parameters indicated a direct relation with ACAD contents, whereas GLTN and MBA showed opposite effects. The pH-responsive nature and degradation rate with the passage of time were investigated by swelling, drug release, and biodegradation studies. The pH-responsive nature of the fabricated hydrogel not only protected the upper parts of the gastrointestinal tract from the drug's adverse effects but also kept the drug away from gastric degradation at the same time. Hydrogel formulations with increasing concentrations resulted in a slow biodegradation of hydrogel networks, further increasing the biocompatibility of the polymeric hydrogel. The excellent cell viability and presence of high live cells after treating with high concentrations of the hydrogel formulation indicated an effective and safe use of the natural polymer-based hydrogel. Overall, the formulated hydrogel can be recommended as an effective applicant for controlled delivery of such drugs, experiencing the same drawbacks as Qn after their administration.

Author contributions

Muhammad Suhail: investigation, data curation, methodology, conceptualization, writing – review and editing and funding acquisition, Abdul Wahab: formal analysis, Guiyue Wang: data curation, Susu An: data curation, Bushra Kiran: data validation, Naila Jabeen: data validation, M. Zubair Iqbal: project administration, supervision, Xiangdong Kong: data curation and validation, Pao-Chu Wu: data curation, validation and funding acquisition.

Conflicts of interest

There are no conflicts to declare.

Data availability

All relevant data are included within the paper.

Acknowledgements

The authors acknowledge the support of the Scientific Research Foundation of Zhejiang Sci-Tech University (23212204-Y) and the National Science and Technology Council of Taiwan (NSTC 112-2320-B-037-014-MY3).

References

1 S. Correa, A. K. Grosskopf, H. Lopez Hernandez, D. Chan, A. C. Yu, L. M. Stapleton and E. A. Appel, *Chem. Rev.*, 2021, **121**, 11385–11457.
2 S. Cascone and G. Lamberti, *Int. J. Pharm.*, 2020, **573**, 118803.
3 A. Mahmood, D. Patel, B. Hickson, J. DesRochers and X. Hu, *Int. J. Mol. Sci.*, 2022, **23**, 1415.
4 M. L. Pita-López, G. Fletes-Vargas, H. Espinosa-Andrews and R. Rodríguez-Rodríguez, *Eur. Polym. J.*, 2021, **145**, 110176.
5 G. Zhou and T. Groth, *Macromol. Biosci.*, 2018, **18**, 1800112.
6 T. D. Carrillo-Castillo, A. Luna-Velasco, E. A. Zaragoza-Contreras and J. S. Castro-Carmona, *e-Polymers*, 2021, **21**, 910–920.
7 M. A. Haghighat Bayan, Y. J. Dias, C. Rinoldi, P. Nakielski, D. Rybak, Y. B. Truong, A. L. Yarin and F. Pierini, *J. Polym. Sci.*, 2023, **61**, 521–533.
8 T. Sarwar, Z. A. Raza, M. A. Nazeer and A. Khan, *Int. J. Biol. Macromol.*, 2024, **256**, 128525.
9 S. R. Batool, M. A. Nazeer, D. Ekinci, A. Sahin and S. Kizilel, *Int. J. Biol. Macromol.*, 2020, **150**, 315–325.
10 M. L. McCain, A. Agarwal, H. W. Nesmith, A. P. Nesmith and K. K. Parker, *Biomaterials*, 2014, **35**, 5462–5471.
11 Y. Jiang, X. Xv, D. Liu, Z. Yang, Q. Zhang, H. Shi, G. Zhao and J. Zhou, *BioResources*, 2018, 13.
12 Q. Xing, K. Yates, C. Vogt, Z. Qian, M. C. Frost and F. Zhao, *Sci. Rep.*, 2014, **4**, 4706.
13 S. M. H. Bukhari, S. Khan, M. Rehanullah and N. M. Ranjha, *Int. J. Polym. Sci.*, 2015, **2015**, 187961.
14 E. J. Cozens, N. Roohpour and J. E. Gautrot, *Eur. Polym. J.*, 2021, **146**, 110250.
15 P. Winstanley and A. Breckenridge, *Ann. Trop. Med. Parasitol.*, 1987, **81**, 619–627.
16 G. Mihaly, M. Ching, M. Klejn, J. Paull and R. Smallwood, *Br. J. Clin. Pharmacol.*, 1987, **24**, 769–774.
17 P. M. Dandagi, S. P. Rath, A. P. Gadad and V. S. Mastiholimath, *Ind. J. Pharm. Educ. Res.*, 2014, **48**, 93–99.
18 S. Kesse, K. O. Boakye-Yiadom, M. A. Farooq, M. Aquib, M. S. Filli and W. Bo, *Res. Pharm. Health Sci.*, 2019, **5**, 101–106.
19 S. Khan and N. Anwar, *Int. J. Polym. Sci.*, 2019, **2019**, 6579239.
20 M. Sohail, S. A. Khan, M. U. Minhas, A. Mahmood, S. A. Shah and S. Mohsin, *Int. J. Biol. Macromol.*, 2022, **215**, 579–595.
21 S. F. Badshah, N. Akhtar, M. U. Minhas, K. U. Khan, S. Khan, O. Abdullah and A. Naeem, *Life Sci.*, 2021, **267**, 118931.
22 E. de Souza Costa-Júnior, M. M. Pereira and H. S. Mansur, *J. Mater. Sci.: Mater. Med.*, 2009, **20**, 553–561.
23 A. K. Moussa, H. A. Abd El-Rahman, R. R. Mohamed and D. H. Hanna, *Biomacromolecules*, 2025, **26**, 341–362.
24 S. Khan and N. M. Ranjha, *Polym. Bull.*, 2014, **71**, 2133–2158.
25 N. A. Peppas and J. J. Sahlin, *Int. J. Pharm.*, 1989, **57**, 169–172.
26 Z. Li, Q. Zhang, Z. Li, L. Ren, D. Pan, Q. Gong, Z. Gu, H. Cai and K. Luo, *Acta Pharm. Sin. B*, 2024, **14**, 2194–2209.
27 S. Huang, Y. Hou, Z. Tang, M. Suhail, M. Cui, M. Z. Iqbal and X. Kong, *Nanotechnology*, 2024, **35**, 365102.

28 P. Nonsuwan, P. P. Phiboonchaiyanan, N. Hirun and P. Kraisit, *Carbohydr. Polym.*, 2023, **321**, 121294.
29 Azizullah, Nisar-ur-Rehman, W. Liu, A. Haider, U. Kortz, M. Sohail, S. A. Joshi and J. Iqbal, *Des. Monomers Polym.*, 2016, **19**, 697–705.
30 L. Wang, Z. Wang, X. Zhang, J. Shen, L. Chi and H. Fuchs, *Macromol. Rapid Commun.*, 1997, **18**, 509–514.
31 M. Karan, R. Chadha, K. Chadha and P. Arora, *Pharmacol. Pharm.*, 2012, **3**, 129–138.
32 A. Asnawi, A. a. Nawawi, R. E. Kartasasmita and S. Ibrahim, *ITB J. Sci.*, 2011, **43**, 43–50.
33 I. Khalid, M. Ahmad, M. Usman Minhas and K. Barkat, *Carbohydr. Polym.*, 2018, **181**, 1169–1179.
34 B. Singh and A. Dhiman, *J. Pharm. Biopharm. Res.*, 2019, **1**, 1–14.
35 A. Ashames, K. Ullah, M. Al-Tabakha, S. A. Khan, N. Hassan, A. Mannan, M. Ikram, M. Buabeid and G. Murtaza, *PLoS One*, 2022, **17**, e0271623.
36 C. S. Ki, D. H. Baek, K. D. Gang, K. H. Lee, I. C. Um and Y. H. Park, *Polymer*, 2005, **46**, 5094–5102.
37 C. D. Bucak, *Cellulose*, 2023, **30**, 1117–1132.
38 C.-T. Lee, C.-P. Huang and Y.-D. Lee, *Biomol. Eng.*, 2007, **24**, 131–139.
39 U. Rehman, R. M. Sarfraz, A. Mahmood, T. Mahmood, N. Batool, B. Haroon and Y. Benguerba, *J. Polym. Res.*, 2023, **30**, 41.
40 N. M. Ranjha, G. Ayub, S. Naseem and M. T. Ansari, *J. Mater. Sci.: Mater. Med.*, 2010, **21**, 2805–2816.
41 S. Bashir, N. Zafar, N. Lebaz, A. Mahmood and A. Elaissari, *Processes*, 2020, **8**, 1350.
42 P. Sarika, N. R. James and D. K. Raj, *Mater. Sci. Eng., C*, 2016, **68**, 251–257.
43 X. B. Hu, *Polym. Bull.*, 2011, **66**, 447–462.
44 A. G. Sullad, L. S. Manjeshwar and T. M. Aminabhavi, *Ind. Eng. Chem. Res.*, 2010, **49**, 7323–7329.
45 L. Ali, M. Ahmad, M. Usman and M. Yousuf, *Polym. Bull.*, 2014, **71**, 31–46.
46 R. W. Korsmeyer, R. Gurny, E. Doelker, P. Buri and N. A. Peppas, *J. Pharm. Sci.*, 1983, **72**, 1189–1191.
47 R. R. Mohamed, M. H. A. Elella and M. W. Sabaa, *Int. J. Biol. Macromol.*, 2015, **80**, 149–161.
48 P. S. K. Murthy, Y. M. Mohan, J. Sreeramulu and K. M. Raju, *React. Funct. Polym.*, 2006, **66**, 1482–1493.
49 M. Sairam, V. R. Babu, B. V. K. Naidu and T. M. Aminabhavi, *Int. J. Pharm.*, 2006, **320**, 131–136.
50 R. Jankaew, N. Rodkate, S. Lamlertthon, B. Rutnakornpituk, U. Wichai, G. Ross and M. Rutnakornpituk, *Polym. Test.*, 2015, **42**, 26–36.